Characterization of functionalized chromatographic mesoporous silica materials: Coupling water adsorption and intrusion with NMR-relaxometry

Carola Schlumberger¹, Carlos Cuadrado Collados¹, Jakob Söllner¹, Christoph Huber², Dorothea Wisser², Hsiao-Feng Liu^{3,4}, Chun-Kai Chang^{3,4}, Stephanie A. Schuster⁵, Mark R. Schure⁶, Martin Hartmann², J. Ilja Siepmann^{3,4}, Matthias Thommes¹*

Corresponding Author

* Matthias Thommes, Institute of Separation Science and Technology, Friedrich-Alexander-Universität Erlangen-Nürnberg, Egerlandstr. 3, 91058 Erlangen, Germany, telephone: +49 9131 8527440, fax: +49 9131 8527441, matthias.thommes@fau.de

¹ Institute of Separation Science and Technology, Friedrich-Alexander-University Erlangen-Nürnberg, Egerlandstr. 3, 91058 Erlangen, Germany

² Erlangen Center for Interface Research and Catalysis (ECRC), Friedrich-Alexander-University Erlangen-Nürnberg, Egerlandstr. 3, 91058 Erlangen, Germany

³ Department of Chemistry and Chemical Theory Center, University of Minnesota, 207 Pleasant St. SE, Minneapolis, MN 55455, United States

⁴Department of Chemical Engineering and Materials Science, University of Minnesota, 421 Washington Ave. SE, Minneapolis, MN 55455, United States

⁵Advanced Materials Technology, 3521 Silverside Road, Suite 1-K, Quillen Building, Wilmington, DE 19810, United States

⁶ Kroungold Analytical, Inc., 1299 W Butler Pike, Blue Bell, PA 19422, United States

Abstract

Silica particles are widely used as a support material for chemically-bound (or bonded) stationary phases in chromatographic separation processes. The tuning of textural properties and surface chemistry of stationary phase materials (SPMs) is crucial to enhance their selectivity to certain compounds and the efficiency of the separation process. Silica supports have the advantage that their surface can be modified with a large variety of hydrophilic and hydrophobic functional groups, but their influence on the silica surface properties has not been evaluated in detail. In this sense, the contact angle is a key parameter for the assessment of surface chemistry but its quantification in a porous matrix is particularly challenging and requires a combination of various tools and experimental techniques. In this work we demonstrate that by combining water adsorption and intrusion measurements it is possible to derive reliable information of the effective contact angle θ of adsorbed water for wetting (θ = 0°), partial wetting ($\theta < 90^{\circ}$), and non-wetting situations ($\theta > 90^{\circ}$) observed on the pore walls of the SPMs under study. By quantitative ¹H solid-state NMR spectroscopy under Magic Angle Spinning, the number of adsorbed water molecules and functional groups per surface area can be estimated. Furthermore, NMR relaxometry experiments reveal that the $T_{1,ads.film}$ / $T_{2,ads.film}$ ratio of relaxation times can be correlated with the effective adsorption strength of water on the surface. Indeed, we find a linear correlation between the negative inverse of the $T_{1,ads,film}$ / $T_{2,ads.film}$ -ratio (i.e., $-T_{2,ads.film} / T_{1,ads.film}$) with the contact angle determined from water vapor adsorption and intrusion experiments for the investigated SPMs. Our work clearly demonstrates for the first time that water vapor adsorption experiments and a novel water intrusion technique coupled with NMR relaxometry can be used as complementary techniques to quantitatively analyze the wettability behavior and surface chemistry of nanoporous materials.

1 Introduction

Chromatography is a widely used technique for the separation of organic and inorganic compounds and substances, e.g., amino acids, proteins, nucleic acids, hydrocarbons, and carbohydrates. Process design and optimization of chromatographic separations requires the tuning of the selectivity of the chromatographic stationary phase material (SPM) in relation to the specific compounds of interest. Porous silica particles are commonly used as SPMs in chromatography column applications. In fact, more than 90% of modern high-performance liquid chromatography (HPLC) columns are packed with porous silica particles due to their good mechanical strength, high chemical and thermal stability, controllable pore structure and surface area, as well as a relatively easy modification with functional groups to induce different polarities [1–3]. Improvements of such SPMs are crucial for process design and optimization in order to achieve an efficient chromatographic separation. Textural properties, such as specific surface area, pore size (distribution), and pore volume may affect selectivity, the transport properties, and, hence, the efficiency of the separation process. In addition, the surface chemistry of the silica plays an important role since it can enhance the affinity and selectivity to certain compounds. Thus, an effective approach for improving the separation efficiency is based on tuning the surface composition of the SPMs. One of the advantages of using silica as SPM is that its surface contains active silanol groups (Si-OH, free OH groups of the silica), which enables the modification of the surface chemistry by grafting different types of functional groups and silanes to create monomeric or polymeric bonded phases. This controllable and tailorable way of modifying the silica surface polarity results in enhancing its utility as SPMs in separation processes. For example, the silica surface is functionalized with hydrophobic compounds, e.g. C8 or C18 chains, for reversed-phase liquid chromatography in order to achieve good retention and high-resolution separation of hydrophobic, usually organic compounds [4–6]. A large variety of different ligands (changing alkyl lengths, including embedded polar groups or aromatic rings, and varying degree o fluorination), is found in bonded-phase chromatography, and the retentive properties of the resulting SPMs are drastically modified depending on the nature of the organic moiety.

Up to now, there is a lack of detailed information on the influence of the bonded ligands on the final textural and chemical properties of the functionalized SPM. A detailed assessment of texture and surface chemistry of porous functionalized stationary phase materials, especially the quantification of the surface chemistry inside the pores is very challenging and requires the combination of different tools [7].

Within this context we suggest here to combine for the first time advanced physisorption and water intrusion techniques with NMR relaxometry to assess important aspects of the surface chemistry (hydrophilicity/hydrophobicity) of SPMs with focus on their hydrophilic/hydrophobic nature.

A useful quantification of the latter is by determining the contact angle of a suitable adsorbed liquid on the surface. For nonporous surfaces, droplet contact angles can be directly obtained by optical and tensiometry methods, e.g., the Wilhelmy technique [8,9] and the sessile drop technique [10]. However, determining the contact angle within the porous matrix is more challenging as the application of the above mentioned macroscopic experimental techniques is not possible to nanoporous materials.

To address this challenge, methodologies based on advanced adsorption have been applied which allow for assessing surface heterogeneity including hydrophilicity/hydrophobicity of the pore walls by using a variety of adsorptives with a wide range of polarities and different interaction strengths with surface functional groups [11–13]. Particularly, the use of water vapor adsorption for surface chemistry and pore structure characterization has been investigated [8,11,14–19]. However the interpretation of water adsorption isotherms is not straightforward as they are affected by both surface chemistry as well as pore size and structure. To differentiate between surface chemistry and textural effects on water adsorption isotherms, it is beneficial to compare the adsorption isotherms with those of completely wetting fluids, which are less sensitive to details of the surface chemistry, e.g. Ar adsorption at 87 K [12]. Coupled with the application of dedicated methods based on non-local-density functional theory (NLDFT), this allows for a reliable assessment of textural properties such as surface area and pore size (pore size/volume distribution). This provides now the basis for deriving reliable information from water adsorption for surface chemistry assessment, but determining the contact angle within the porous matrix is more challenging as the application of the above mentioned macroscopic experimental techniques on nonporous surfaces. A suitable approach relies on deriving the contact angle of water on pore surfaces based on water adsorption in combination with the Kelvin equation if the pore size (and pore size distribution) is known [14,15,18,20]. However, the determination of the correct equilibrium contact angle from water sorption isotherms, which often exhibit hysteresis, requires a detailed understanding of the contributions to hysteresis and can, contrary to the work presented in these papers, not be calculated from the adsorption branch. In fact, the choice of adsorption branch for deriving the contact angle is not straightforward, because the pressure where pore condensation/filling occurs is delayed due to metastable pore fluid (i.e., nucleation barriers associated with condensation/pore filling), while the desorption branch of the hysteresis loop reflects in the absence of pore network effects (e.g., pore blocking, cavitation) the liquid-vapor equilibrium transition, and hence is better suited as the basis for assessing the effective, equilibrium contact angle of an adsorbed water phase [21].

However, the application of this methodology is limited to wetting and partially wetting surfaces with a contact angle θ between 0° and 90° . We therefore combine the water vapor adsorption experiments with water intrusion/extrusion experiments for non-wetting surfaces ($\theta > 90^{\circ}$). In this case, the contact angle can be determined with the Washburn equation [21] by applying hydraulic pressure to force the water inside of the pores.

In addition to water vapor adsorption and water intrusion experiments, we have shown that NMR relaxometry measurements can be a complementary tool for the fast assessment and quantification of the surface chemistry of nanoporous materials. We have shown recently that the ratio of spin-lattice (T_1) and spin-spin (T_2) relaxation time $(T_1/T_2$ -ratio) is characteristic for the wetting behavior of adsorbates on silica and carbons surfaces [22]. The relaxation time ratio has been used in the petrochemical industry to analyze the wetting behavior of oil in sedimentary rocks, e.g. [23,24]. In addition, it was demonstrated that the T_1/T_2 -ratio of catalysts in contact with different liquids can be associated with the effective interaction strength between these liquids and the catalyst surface [25–27]. Furthermore, these measurements indicated a linear correlation between the negative inverse relaxation time ratio $(-T_2/T_1)$ of different porous materials with the adsorption energy E_{ads} determined from temperature programmed desorption (TPD) experiments [28–30]. However, the specific surface area of the material under study may also affect the T_1/T_2 ratio as the specific surface area has a stronger effect on T_2 relaxation compared to T_1 relaxation [22,31]. In order to address this problem, we therefore suggest here to use the ratio of specific surface relaxivities $(k_{a,2}/k_{a,1})$ as an indicator for surface chemistry effects as this value is similar to the relaxation time ratio $T_{1,ads,film}/T_{2,ads,film}$ of the adsorbed liquid film on the pore surface and, hence, independent of the specific surface area of the material under study and solely affected by the surface chemistry. This comprehensive surface chemistry assessment presented in this study is complemented by solidstate NMR spectroscopy under Magic Angle Spinning (MAS) condition. By ¹H MAS NMR spectra, the resonances of adsorbed water, silanol groups and organic functional groups were assigned for three samples. Absolute quantification of the number of ¹H spins by external calibration allowed to estimate the number of adsorbed water molecules, the number of functional groups and the number of end-capping groups per nm² of support surface.

In this work we demonstrate the applicability of this combined powerful experimental toolbox for both the textural and surface chemistry characterization, with a focus on hydrophibicity/hydrophilicity, on mesoporous silica materials, either in the pristine state or functionalized with four different organic moieties, which are commercially used as SPMs in chromatography. The functional groups used to modify the surface chemistry are illustrated in Scheme 1. We demonstrate that it is possible to derive, by combining water adsorption and intrusion experiments reliable information of the effective contact angle θ of adsorbed water for wetting ($\theta = 0^{\circ}$), partial wetting ($\theta < 90^{\circ}$), and non-wetting situations ($\theta > 90^{\circ}$) observed on the pore walls of the SPMs under study. Further, NMR relaxometry measurements of selected SPMs immersed in water reveal that the $T_{1,ads.film}/T_{2,ads.film}$ -ratio can be correlated with the effective adsorption strength of water on the surface. Indeed, we find a linear correlation between the negative inverse of the $T_{1,ads.film}/T_{2,ads.film}$ -ratio (- $T_{2,ads.film}/T_{1,ads.film}$) with the contact angle determined from water vapor adsorption and intrusion experiments for the investigated SPMs. Our work clearly demonstrates for the first time that water vapor adsorption experiments and novel water intrusion technique coupled with NMR relaxometry can be used as complementary techniques to quantitatively analyze the wettability behavior and surface chemistry of nanoporous materials.

2 Material and Methods

In this work, five commercially available stationary phase silicas with different bonded ligands obtained from Advanced Materials Technology (AMT) were investigated as shown in Scheme 1Error! Reference source not found.: Pristine silica (AMT silica), silica functionalized with dimethyloctadecylsilane (AMT C18), silica functionalized with dimethyloctylsilane (AMT C8), silica functionalized with dimethyl pentafluorophenylpropylsilane (AMT PFP), and silica functionalized with glycan (AMT glycan). The AMT SPMs are superficially-porous (Fused-Core®) particles where a non-porous core (diameter of $\approx 1.7 \, \mu m$) is surrounded by a shell formed by smaller spherical silica nanoparticles (diameter of $\approx 10 \, nm$). The interstitial region between the nanoparticles yields a porous network [32]. The surface chemistry of each SPM is different based on the bonded ligand on its surface. Scheme 1 shows an overview of the silica SPMs and their corresponding bonded ligands.

Scheme 1: Evaluated functionalized silica SPMs: a) dimethyloctadecylsilane (C18), b) dimethyloctylsilane (C8), c) pentafluorophenylpropylsilane (PFP), d) glycan functionalization

2.1 Textural characterization by gas adsorption

High-resolution gas adsorption measurements were performed on a commercial Autosorb iQ automatic volumetric adsorption analyzer from Anton Paar (QuantaTec, Boynton Beach, FL, USA) equipped with 1, 10 and 1000 Torr transducers. *AMT silica* was degassed at 150 °C for 12 h under vacuum prior to all gas adsorption experiments. The functionalized SPMs were degassed at 120 °C for 12 h under vacuum in order not to modify the surface chemistry due to removal or degradation of the bonded ligands. Textural properties were analyzed using a combination of argon (Ar 6.0 purchased from AirLiquide) at T = 87 K and nitrogen at T = 77 K adsorption experiments. Argon isotherms were measured in a relative pressure range of approx. 10^{-5} up to 1 for each material. Network characteristics of the SPMs were analyzed by comparing the pore size distributions determined from the adsorption and desorption branches of the material using a dedicated metastable and equilibrium non-local density functional theory (NLDFT) kernel assuming cylindrical pores that appears to be the best match for the complex mesopore network in the shell of the superficially-porous particles.

2.2 Investigation of surface chemistry by water vapor adsorption experiments

The evaluated SPMs can be classified depending on their surface chemistry and interaction with water as hydrophilic and hydrophobic (high and low water affinity, respectively). For the first

case, water pore filling takes place at pressures below water's saturation pressure ($p < p_0$), whereas for the second one, water must be forced to get into the pores by applying pressures highly above saturation pressure ($p > p_0$). Thus, two experimental methodologies were used to determine the effective contact angle: water adsorption isotherms for hydrophilic silica and water intrusion measurements for hydrophobic silica.

Water adsorption experiments were performed at 298 K with a dedicated volumetric (manometric) vapor sorption analyzer Vstar (Anton Paar QuantaTec) in the relative pressure range of $p/p_0 = 0.005$ up to 0.99. AMT silica was degassed at 150 °C, while the functionalized SPMs were degassed at 120 °C for 12 h under vacuum prior to the adsorption experiments.

Water adsorption experiments were performed on a fresh sample from the same homogeneous batch that was used for Ar adsorption experiments. A second cycle (without any additional thermal treatment) was measured for the same sample in order to evaluate the hydroxylation of the surface after the first cycle.

2.3 Investigation of surface chemistry by water intrusion measurements

The determination of the contact angle of water on non-wetting surfaces ($\theta > 90^{\circ}$) is based on water intrusion/extrusion experiments. Water intrusion experiments were performed using a Poremaster 60 (Anton Paar, Germany) and sealed polymer envelopes, containing water and the hydrophobic C18 silica. For the preparation of the polymer envelopes, highly purified water with a conductivity of 0.060 mS m⁻¹ was degassed with helium for at least 5 minutes. The porous material was then introduced into a prepared polymer envelope. Additionally, water in a large excess compared to the mesopore volume was carefully pipetted into the envelope. Finally, the envelope was sealed under vacuum. The vacuum was drawn until the boiling pressure of water (ambient temperature) was reached. After that, the sample was introduced into the cell of the mercury porosimeter. All measurements were performed using the smallest motor speed in the autospeed mode. For the high-pressure measurements, starting at 20 psi, 2 cycles were always measured. All intrusion measurements were performed at room temperature (≈ 25 °C).

The polymer envelope and water both show significant compressibility effects upon pressurization. Therefore, we apply a compressibility correction. The compressibility of the polymer is accounted for by a reference measurement, in which solely the polymer envelope is pressurized in the porosimeter. The compressibility of water is accounted for by utilizing the bulk modulus of water at 25 °C, calculated via the density and the speed of sound [33]. Detailed information about the compressibility correction is provided in the Supporting Information. During preparation of the polymer envelope, the mass of the polymer and water is recorded. This mass is used to scale the reference curves of water and polymer accordingly to obtain a compressibility corrected water intrusion curve.

2.4 Surface chemistry investigation by NMR relaxometry and spectroscopy

The surface chemistries of three SPMs with a range of hydrophilicities (*AMT silica*, *AMT glycan* and *AMT C18*) were investigated based on the $T_{I,ads,film}/T_{2,ads,film}$ -ratio determined from NMR relaxometry experiments via the ratio of specific surface relaxivities ($k_{a,2}/k_{a,1}$). For this, the SPMs were immersed in deionized water (Millipore water made with a PURELAB flex 2 by ELGA LabWater) prior to NMR relaxation measurements at a concentration of approx. 20 wt%. The SPMs were left in water for at least 24 h to ensure complete hydroxylation of the surface. Homogeneous suspensions were prepared by mixing the samples in an ultrasonic bath (Branson 1510) for 2 h and stirring for 30 min at approx. 700 rpm.

For AMT silica and AMT glycan, both samples were left until the particles formed a clearly visible sediment and the excess liquid was removed with a pipette. Additional excess bulk water

was removed by keeping the samples in a drying oven at 80 °C for 30 min. Afterwards, the samples were immediately transferred to 10 mm NMR tubes (Bruker) and relaxation times were measured with a benchtop NMR device (Bruker minispec mq20). The temperature of the device was stabilized at 25 °C during the measurements. The inversion recovery pulse sequence was used for the determination of the spin-lattice relaxation time T_I . The Carr-Purcell-Meiboom-Gill (CPMG) pulse sequence was used for the determination of the spin-spin relaxation time T_2 (see the Supporting Information for more details).

For the AMT C18 sample, a fast separation of the water and solid powder was visible due to the hydrophobic nature of this SPM. In this case, the solid powder was swimming on top of the liquid water phase as soon as the stirring stopped. This upper powder was transferred to a 10 mm NMR tube and relaxation times were measured in the same way as for the more hydrophilic SPMs. In this case, water molecules will most likely not be inside of the pores but between the particles. However, as we assume the external surface chemistry to be identical to the internal surface chemistry, the $T_{1,ads,film}/T_{2.ads,film}$ -ratio can still be used as a measure of surface chemistry effects.

For all 3 samples, the weight of the water-saturated solid powder in the NMR tube was determined. After the NMR measurements, the samples in the NMR tubes were degassed under vacuum at 150 °C for 12 h by connecting the NMR tubes to a Xeriprep (Anton Paar). Finally, the weight of the dry powder was determined after degassing.

Solid-state MAS NMR spectra were acquired on a 500 MHz (11.7 T) DD2 Varian spectrometer at a ¹H resonance frequency of 499.86 MHz. Samples were activated at 150 °C (*AMT silica*) / 120 °C (functionalized SPMs) and packed into 1.6 mm zirconia rotors under argon atmosphere. An MAS rate of 20 kHz was used. For background suppression, a DEPTH sequence was applied, consisting of a 90 ° pulse (100 kHz) followed by two 180 ° pulses (100 kHz) with a combined CYCLOPS and EXORCYCLE phase scheme [34–36]. 16 scans were accumulated. Spectra were deconvoluted using DMFit [37].

To obtain a calibration of the signal intensity vs. absolute number of ¹H nuclei in a sample, we used the external calibration which we have introduced previously [38]. KBr was finely ground and dried at 150 °C overnight. The freshly dried KBr was mixed with adamantane in five different ratios (0.003 g, 0.006 g, 0.010 g, 0.050 g and 0.100 g adamantane per 1.0 g of mixture) under ambient conditions. The spectra were acquired immediately after preparation. From the sample mass in the rotors and the absolute integrals of the respective ¹H NMR signal, a linear calibration curve for quantitative ¹H assessment was obtained (see Figure S3).

3 Results and Discussion

3.1 Textural characterization

A comprehensive textural characterization of *AMT silica* as well as the functionalized AMT materials was obtained by an advanced gas adsorption methodology based on a combination of argon 87 K and N₂ 77 K (see Figure 1a) in combination with pore size/volume analysis by applying a dedicated non-local density functional theory (NLDFT) method (Figure 1

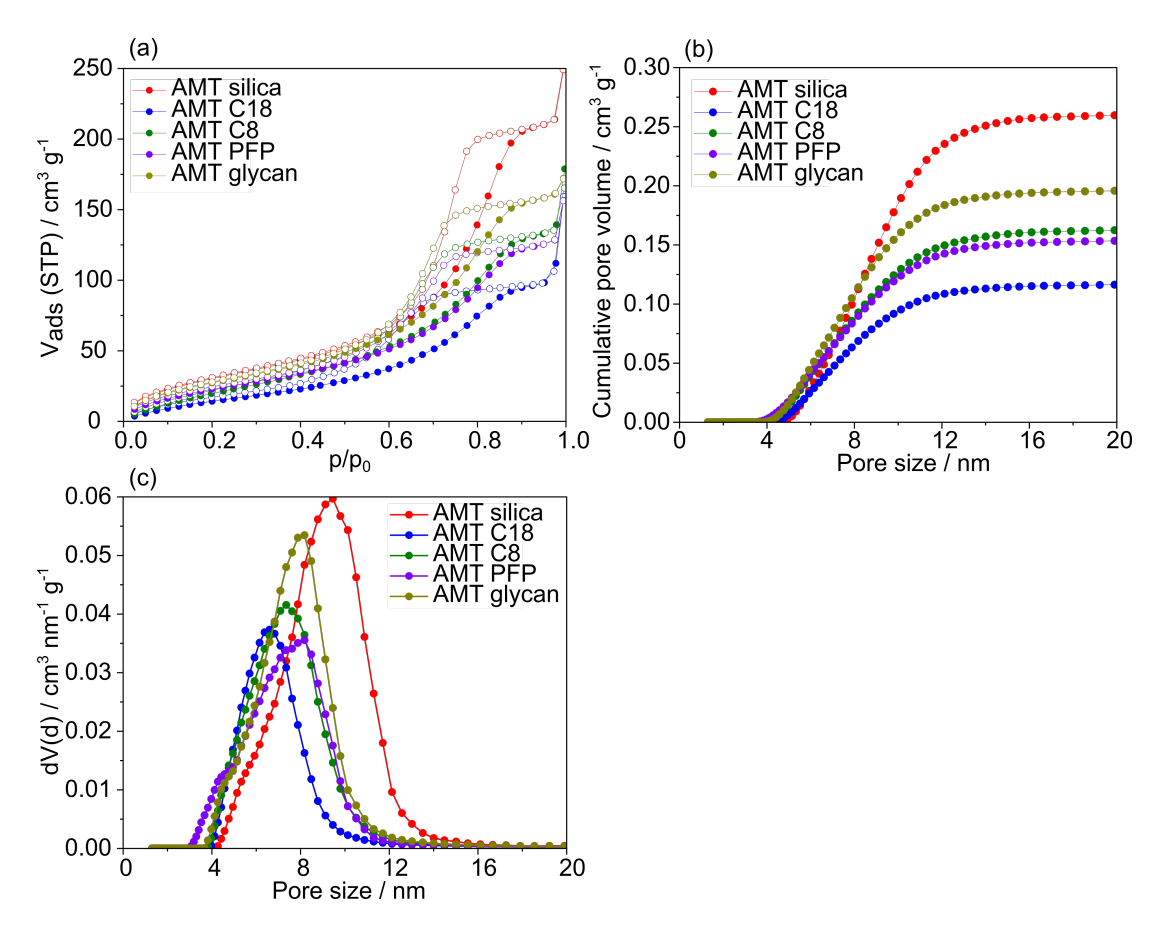


Figure 1: a) Ar 87 K adsorption isotherms for the evaluated SPMs. Full symbols represent the adsorption branch and open symbols represent the desorption branch. b) Cumulative pore volume and c) Differential pore size distribution obtained by applying a dedicated NLDFT cylindrical equilibrium kernel to the desorption branch.b and Figure 1c) assuming cylindrical pores. All samples exhibit a type IVa isotherm characteristic of mesoporous materials [39]. The shape of the hysteresis, which can be classified as a combination of H1 and H2 type (the adsorption—desorption branches are not completely parallel), suggests that the majority of mesopores are freely accessible to the external surface without restrictions, but still a fraction of larger mesopores is restricted by smaller pores (ink-bottle pores) [39]. A detailed analysis and comprehension of the pore network and connectivity is provided below.

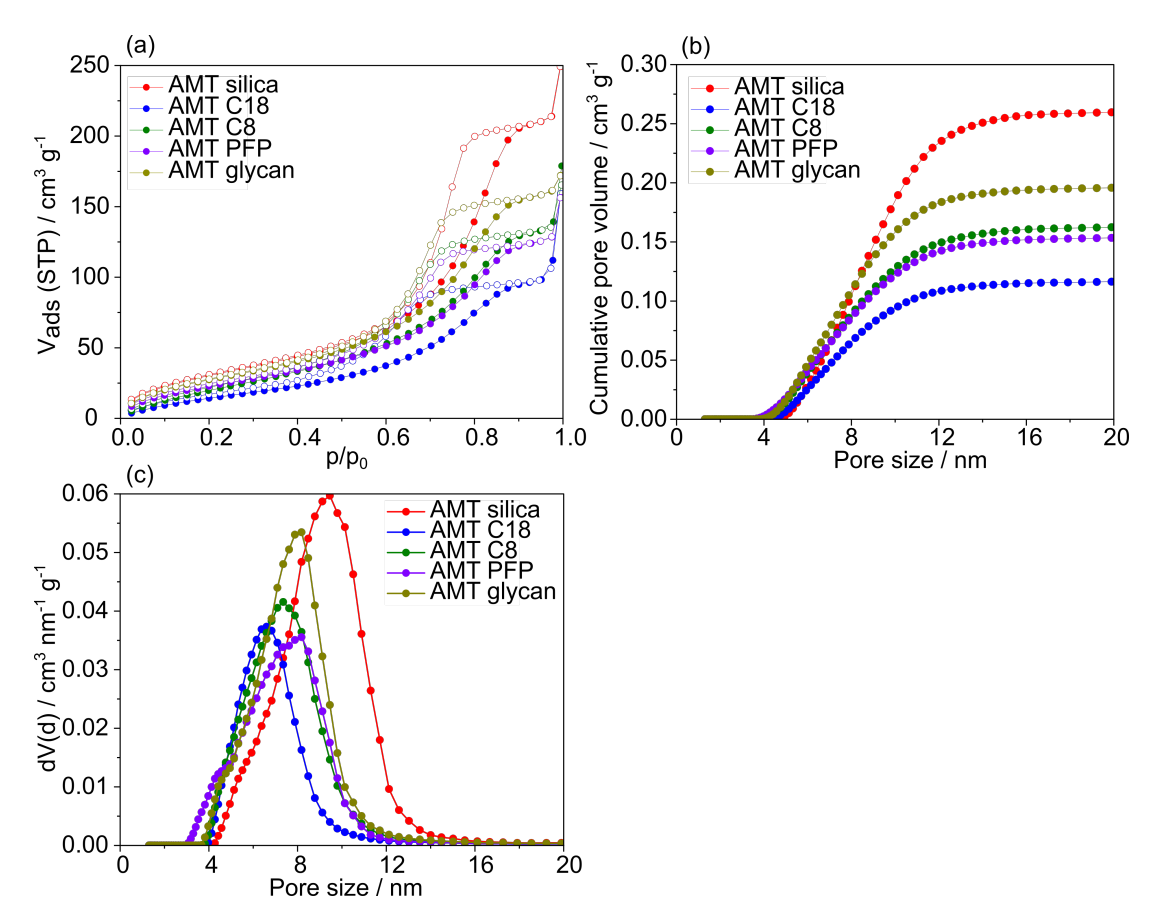


Figure 1: a) Ar 87 K adsorption isotherms for the evaluated SPMs. Full symbols represent the adsorption branch and open symbols represent the desorption branch. b) Cumulative pore volume and c) Differential pore size distribution obtained by applying a dedicated NLDFT cylindrical equilibrium kernel to the desorption branch.

Figure 1b shows the cumulative pore volume for the five samples. The negligible pore volume below 2 nm indicates that these SPMs do not possess any microporosity. *AMT silica* has the highest Ar uptake, thus leading to the largest total pore volume. The pore size distribution for this material is rather broad with mesopores in the range between 5 and 17 nm. However, the complexity of the pore network (e.g., different local pore shapes) in the shell of the superficially porous particles may contribute to the broadness of the pore size distribution. The incorporation of the bonded ligands into the silica leads to a clear decrease of the pore volume but also of the mesopore size. For the latter case, a clear shift of the mean mesopore size can be observed in the pore size distribution (Figure 1c) for all functionalized SPMs compared to *AMT silica* (calculated from the desorption branch). As mentioned before, the hysteresis helps to understand the pore connectivity of a material by evaluating the vapor—liquid phase transition in the adsorption/desorption process. For this analysis, pore size distributions were calculated from the Ar 87 K adsorption branch using a dedicated NLDFT metastable adsorption kernel and from the Ar 87 K desorption branch using a dedicated NLDFT equilibrium kernel (see Figure 2Error! Reference source not found.a [40,41].

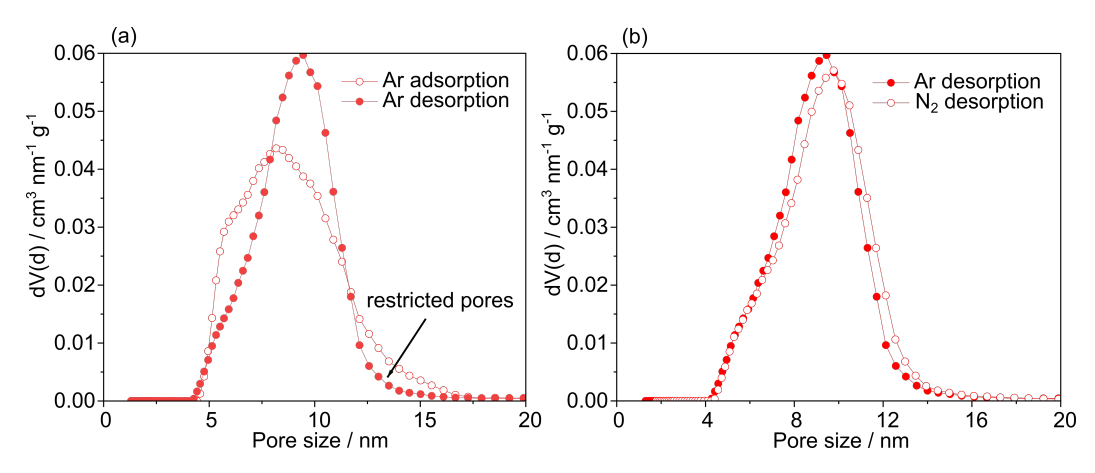


Figure 2: Differential pore size distribution a) using a dedicated NLDFT metastable kernel and equilibrium kernel to the Ar at 87 K adsorption and desorption branch, respectively and b) using a dedicated NLDFT equilibrium kernel to the Ar 87 K and N_2 at 77 K desorption branch

Two features can be clearly distinguished in the pore size distributions. Firstly, for pores smaller than 9 nm, a small shift of the pore size distribution determined from the adsorption branch to smaller pore sizes is observed compared to the pore size distribution from the desorption branch. Such shift can be attributed to initiated/advanced condensation, i.e. the effective nucleation barrier associated with the nucleation of the liquid phase is reduced in an interconnected pore network resulting in a phase transition at a relative pressure smaller than the corresponding relative pressure with the spinodal of the fluid in these pores [40]. The occurrence of initiated condensation is known to exist in highly connected 3D pore networks [42,43], and it is expected for the superficially porous particles investigated here. For pores smaller than 9 nm, the desorption branch reflects thermodynamic equilibrium and the pore size can be determined in a straightforward way from the desorption branch. On the other hand, for pores larger than 12 nm, a shift of the pore size distribution determined from the desorption branch to smaller pore sizes can be observed, meaning that such larger cavities empty via pore blocking. Taking into account that in this complex 3D pore network system, during adsorption the pores are filled prior to the spinodal (initiated condensation), whereas during desorption most of the pores empty in an equilibrium liquid to vapor transition (only a small fraction of large pores empty via pore blocking), the pore size distribution can be reliably determined from the desorption branch of the N₂ 77 K and Ar 87 K isotherms (under the assumption of predominantly cylindrical pores). The confirmation of the emptying of such large mesopores by pore blocking is shown in Figure 2b. Since the pressure at which evaporation occurs is ruled by the size of the necks, the pore size distribution determined from the desorption branch is independent of the chosen adsorptive [40] and indeed, Error! Reference source not found.b exhibits a very good agreement of the pore size distributions obtained from Ar 87 K and N₂ 77 K desorption branches.

Molecular simulations were carried out on model systems with non-standard pore geometries to provide further insight into the pore filling mechanism (see Supporting Information for the simulation details). A relatively good match with the experimental Ar adsorption isotherm on *AMT silica* was found for a system containing a missing cylinder in an array of hexagonally packed cylinders of amorphous silica, forming small and large pores with the diameter of the large pore being 9 nm (see Figure 3). At low pressure (panel A), the Ar atoms adsorb first onto the corners of small and large cavities. As the pressure increases, the smaller cavity is filled (panel B) before the system reaches the monolayer capacity given by the BET method (panel C) indicating that the BET surface area analysis may overpredict the probe-accessible surface area. At the intermediate pressure range, the shape of the cross-sectional area of the cavity gradually turns from a hexagon to a circle (panels D and E). This behavior is driven by the

liquid—vapor surface tension that leads to the Ar multi-layer to arrange in a manner that reduces the surface area. The simulated isotherm shows a sharp step, indicating that the pore size distribution of the model is narrower than for the AMT silica. Overall, the agreement between the simulated and the experimental isotherms at the low and intermediate pressure range points to contributions from non-convex pore shapes for capturing the adsorption behavior. The hysteresis in the simulated adsorption/desorption branches is wider than that in the experimental measurements (see Supporting Information) because there is no receding meniscus in the infinitely-long model pore.

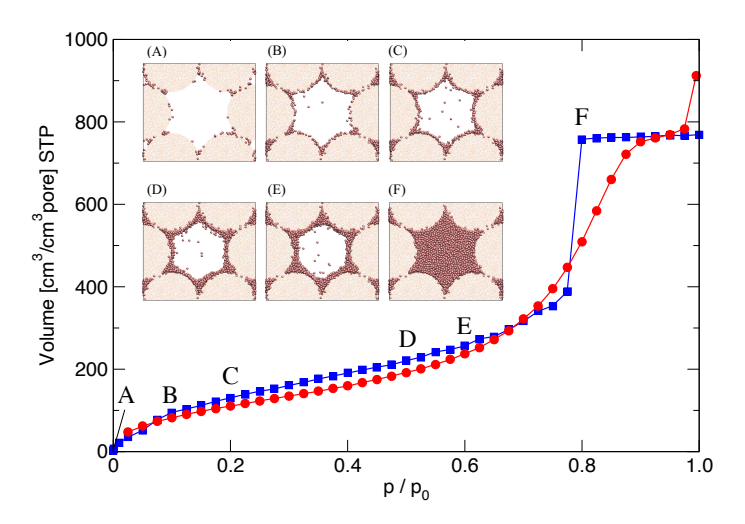


Figure 3: Simulated (blue squares) and experimental (red circles) Ar adsorption isotherms. The inset shows snapshots at reduced pressures of 0.01 (A), 0.1 (B), 0.2 (C), 0.5 (D), 0.6 (E), and 0.8 (F); Ar atoms are depicted as pink spheres; amorphous silica is depicted as points with silicon in yellow and oxygen in red.

Table 1 summarizes the textural properties of the three samples. The BET surface area was calculated by taking a relative pressure range between 0.05 and 0.3 and assuming a cross sectional area of 0.142 and 0.162 nm² for Ar at 87 K and N₂ at 77 K, respectively. The pore volume was determined with NLDFT from the Ar and N₂ adsorption isotherms.

Table 1: Summary of the textural properties of the evaluated SPMs

SPM	$S_{BET~Ar~87K} / m^2 g^{-1}$	$S_{BET N2 77K} / m^2 g^{-1}$	Pore volume Ar 87K / cm ³ g ⁻¹	Pore volume N2 77K / cm ³ g ⁻¹
AMT silica	109	128	0.26	0.26
AMT C18	60	61	0.12	0.12
AMT C8	89	91	0.16	0.16
AMT PFP	87	92	0.15	0.15
AMT glycan	93	104	0.20	0.20

Table 1 reveals a clear effect of the surface chemistry of the different SPMs when comparing the BET surface area determined with Ar and N_2 adsorption on the polar and non-polar surfaces. While the surface areas obtained from Ar and N_2 isotherms give similar values on non-polar SPMs (AMT C18, AMT C8, AMT PFP), a large difference can be observed for polar surfaces (AMT silica and AMT glycan). In the last decades, N_2 was always considered as the standard

adsorptive for the textural characterization of nanoporous materials. However, more recently it was recognized that N₂ has some limitations in its use, primarily due to its molecular quadrupole moment and lone-pair electrons, which leads to specific interactions with polar surface functional groups or exposed ions on material surfaces. These specific interactions between the N₂ molecule and the material's surface can lead to different preferred orientations of the N₂ molecule on the surface of polar materials leading to uncertainty in the cross-sectional area used for BET surface area calculations. In fact, this uncertainty in the assumed cross-sectional area can result in a reported N₂ BET surface area which differs from the true surface area of the material by as much as 20 % if the standard cross-sectional area of 0.162 nm² is used for N₂ [39,44]. In contrast, argon is the recommended adsorptive for surface area determination by IUPAC. First, Ar is monoatomic and, therefore, does not possess rotational degrees of freedom nor any preferred orientations on the surface of the material. This allows for unambiguity in the cross-sectional area of Ar used for surface area calculations. Also, Ar lacks a permanent multipole moment, thus it eliminates first-order electrostatic interactions with any surface functional groups or exposed ions present in these materials. As a result, since there are no firstorder electrostatic or hydrogen-bonding interactions depending on the material's surface chemistry, there is nearly a direct correlation between the Ar pore filling pressure and the pore size of the material.

3.2 Surface chemistry

The comprehensive detailed analysis of the surface chemistry of the five investigated SPMs will be shown in the following by combining water vapor adsorption experiments with water intrusion/extrusion and NMR relaxometry measurements.

3.2.1 ¹H Solid-state NMR spectroscopy

The surface structure of all five samples was further analysed by ¹H solid-state MAS NMR spectra (Figure 4). In AMT silica, after activation, a main resonance at 1.8 ppm can be attributed to isolated silanol groups at the surface. At the same time, a smaller signal of adsorbed water can be found between 2.4 and 4.5 ppm [45]. The bonded-phase samples were activated only under mild conditions at 120 °C in order to avoid thermal degradation of the ligand grafting. This relatively low activation temperature yields a small residual amount of adsorbed water. In the ¹H MAS NMR spectrum of AMT C18, the resonance of isolated silanols is not detectable any more in the precision limits of MAS NMR, showing that these groups have been almost completely replaced by alkyl grafting. In AMT C8, silanol groups are still visible at 1.8 ppm. Signals at 0.9 and 0.7 ppm in both samples can be attributed to CH₂ groups and terminal CH₃ group belonging to the C8 and C18 alkyl chains. Furthermore, a signal around 0 ppm can be seen in all functionalized samples and is attributed to superimposed signals of the CH₃ group directly linked to the silicon atom and to trimethylsilyl (TMS, -Si-(CH₃)₃) groups which have been introduced into the materials to passivate the majority of the remaining isolated surface silanols which are not substituted by C8 or C18 chains (so-called end-capping). Unambiguous attributions of the signals of AMT PFP and AMT glycan were not possible here due to the strong overlap of the signals.

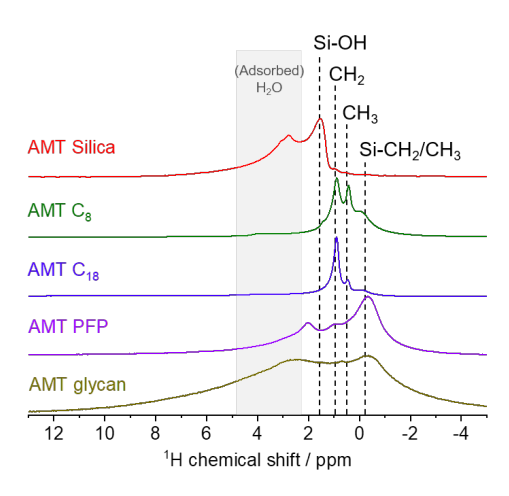


Figure 4: Normalized ¹H MAS NMR spectra acquired on AMT Silica, AMT C8 and AMT C18

The spectra shown in Figure 4 are normalized, their respective relative intensities can be found in the SI (Figure S4). The ¹H NMR spectra were evaluated quantitatively with the help of a ¹H spin density calibration introduced by us recently [38]. The method is based on an external calibration of ¹H spins per mass by a number of samples with known ¹H density, prepared by mixing adamantane with dry KBr. The signals were deconvoluted with Gaussian fits (Figure S5). The results are shown in Table 2. The number of surface groups per nm² was calculated by referencing to the surface area of the pristine material, namely 109 m²g⁻¹, since the ligands were grafted to the pristine silica material post-synthetically. The AMT silica possesses 4.3 isolated silanols per nm² on the surface, which is in good correlation to comparable silica materials from literature [46]. Based on the ¹H spin density calibration, AMT C8 and AMT C18 are estimated to contain 1.2 and 1.4 long-chain alkyl ligands, respectively, and 1.0 and 0.5 endcapping TMS groups per nm², respectively. AMT C8 still exhibits 1.1 isolated silanol groups per nm². These values are close to, but not in accordance with surface coverages obtained by elemental analysis, which indicates surface coverages of approximately 3.7 µmol/m² (2.2) groups per nm²) for the long-chain alkyl ligands and 0.5 μ mol/m² (0.3 groups per nm²) for the TMS end-caps. We note that closely overlapping resonances of CH₂ and CH₃ groups of alkyl chains and TMS end-capping groups prevent an unambiguous deconvolution of the signals. which may impact the relative ratio of long-chain alkyl and TMS groups. A broad signal between 2 and 9 ppm is attributed to hydrogen-bonded silanol groups [46]. This resonance additionally overlaps with the alkyl resonances of the C₈ alkyl grafting (Figure S5). Finally, since the density of long chain alkyl groups was obtained from elemental analysis before TMS grafting, the final density of the former can be somewhat lower if alkyl chains are cleaved during the end-caping process. The number hydrogen bonded silanol groups varies strongly from one sample to another under the given sample preparation conditions. Samples were dried at a relatively low temperature (120 °C) to prevent degradation of the surface functional groups, and may therefore contain residual amounts of adsorbed water, which may also form hydrogenbonds to surface silanol groups. Note that silanols groups which were found to be isolated in the pristine silica material may be engaged in hydrogen bonds. This may explain why no residual isolated silanol signals are observed in C₁₈-grafted silica.

Table 2: Quantitative surface group assignment from ¹H MAS NMR on AMT Silica, AMT C8 and AMT C18.

SPM	H-bonded Si-OH / nm²	Isolated Si-OH / nm ²	Functional groups/ nm ²	Endcapping Si-(CH ₃) ₃ / nm ²
AMT Silica	13.4	4.3	-	-

AMT C8	16.3	1.1	1.2	1.0
AMT C18	10.8	-	1.4	0.5

3.2.2 Water vapor adsorption

Surface chemistry can be assessed by the comparison of adsorptives exhibiting different wettability. For argon, the wall-argon interactions are stronger than the argon-argon interactions leading to a complete wetting adsorbate (effective contact angle is zero) independent of the surface chemistry. However, water adsorption is sensitive to the underlying surface chemistry because water-water interactions by themselves are strong. In fact, the water adsorption mechanism involves the formation of clusters, which form at the most favorable surface sites of the material. If the surface density of very favorable adsorption sites is low, then such clusters continue to grow and generating bigger droplet agglomerates that eventually coalesce. By contrast, argon adsorption proceeds through an adsorbed layer along the surface prior to capillary condensation. Therefore, the effect of the silica SPM surface chemistry was evaluated by measuring water adsorption isotherms at 298 K (Figure 5a).

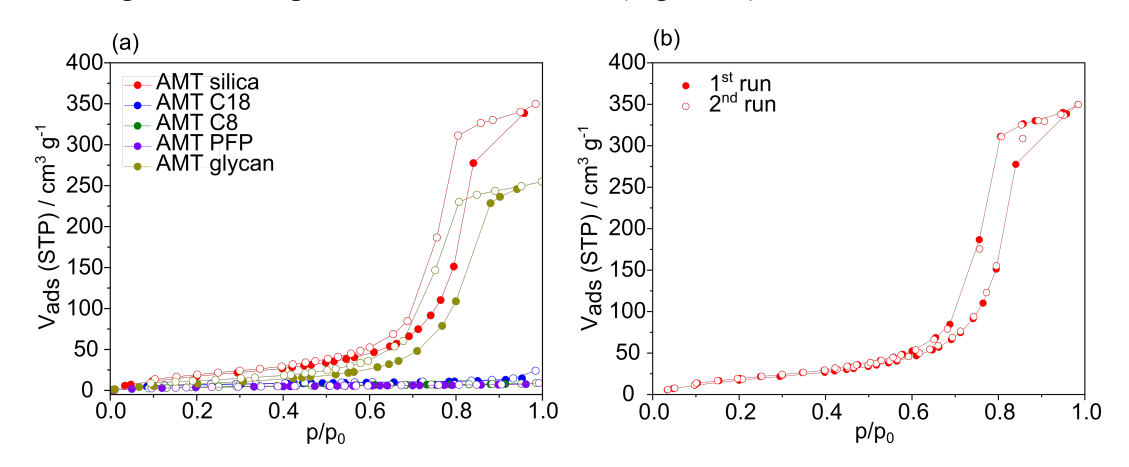


Figure 5: (a) H_2O adsorption-desorption isotherms at 298 K on pristine and bonded-ligand silica SPMs. Full symbols represent adsorption branch and open symbols represent desorption branch. (b) H_2O cyclability at 298 K for AMT silica. Full symbols represent the first cycle and open symbols represent the second cycle.

The measured water isotherms confirm as before mentioned that water adsorption on porous materials does not only depend on the pore volume and pore size but specially on the surface chemistry, thus water is only strongly adsorbed at the active and most favorable sites. For the case of silica SPMs, such active sites correspond to silanol groups on the surface (Si-OH) or hydroxyl, ether, or amide functional groups of the bonded ligand (e.g., AMT glycan). AMT silica and AMT glycan show a type IVa isotherm with a complete mesopore filling due to their high OH content. It should be noted that the density of favorable water adsorption sites on these surfaces is sufficiently high that water adsorption does not have to proceed via the cluster/droplet agglomerate mechanism but involves the formation of a water layer. On the contrary, AMT C8, AMT C18, and AMT PFP show only a very low water uptake since the hydroxyl groups on the surface have been mostly replaced by hydrophobic ligands (C8, C18 and PFP respectively). Even though the overall silica samples exhibit similar surface area and significant mesopore volume based on Ar 87 K adsorption measurements, water can only fill completely the pores of polar materials (AMT silica and AMT glycan), whereas no pore filling is observed at pressures up to the bulk saturation pressure of water.

The silanol content of a pristine silica surface varies depending on many factors such as the synthesis conditions, temperature of calcination, post synthesis treatment, (e.g., silica exposed to a water saturated environment). Thus, water sorption isotherms on pristine silica materials

can look very different depending on such silanol groups. In this sense, previous works on pristine SBA-15 and MCM-41 silica demonstrated that water adsorption measurements resulted in the hydroxylation of the surface during the first water cycle [17]. However, for *AMT silica*, **Error! Reference source not found.**5b clearly shows that no re-hydroxylation of the surface takes place during the first cycle of the water adsorption measurement, which is reflected in the perfect agreement of the adsorption and desorption branch at low relative pressures and the good reproducibility of the first cycle in following cycles. Hence, the *AMT silica* sample was already completely hydroxylated in the beginning of the measurement.

The determination of the effective contact angle of water within the pores from water adsorption measurements on (partially) wetting silica (contact angle < 90°) was done by utilizing the Kelvin equation (eq. 1) which correlates the pressure where the equilibrium vapor—liquid phase transition occurs with the pore diameter (under the assumption of a cylindrical pore geometry).

$$\ln\left(\frac{p}{p_{sat}}\right) = \frac{2\gamma V_L \cos\theta}{(r - t_m)RT} \tag{1}$$

where γ is the bulk surface tension of water, $V_{\rm L}$ is the bulk molar volume of water, θ is the contact angle of water on the silica pore walls, r is the pore radius obtained from the argon sorption measurements, R is the universal gas constant, T is the temperature of the isotherm and $t_{\rm m}$ corresponds to the statistical thickness of the adsorbed water layer. Hence, based on the known textural properties the effective contact angle can be calculated.

For this calculation, the pore radius was previously obtained by applying the BJH method to the desorption branch of the argon 87 K data. The multilayer thickness formed prior to capillary condensation was determined by applying the generalized Halsey equation, (eq. 2) to a reference nonporous silica material (a controlled pore silica glass, Schott) with similar surface composition to the evaluated silica:

$$t_m = a \left(\frac{1}{\ln\left(\frac{p_0}{p}\right)} \right)^{1/b} \tag{2}$$

where a and b are characteristic constants for the given adsorption system and temperature. Such parameters were determined from the controlled pore silica glass and used for the AMT silica. For the case of water, the thickness was calculated by assuming a fully hydroxylated surface on the silica materials.

The generalized Halsey equation was applied to the multilayer region in the p/p_0 range of 0.2-0.7 and 0.2-0.8 for argon and water sorption, respectively, to determine the thickness of the evaluated silica. Lastly, p/p_0 from eq.1 was chosen at the inflection point of the water desorption branch corresponding to the mode of the pore size distribution.

Effective contact angles on AMT silica and AMT glycan from water sorption measurements were found to be ca. 3° and ca. 34°, respectively. As expected, pristine silica shows a contact angle very close to 0°, indicative of a fully wetting surface, due to the highly hydrophilic surface character of the silica. Interestingly, AMT glycan shows a contact angle substantially higher despite the fact that this silica is functionalized with a hydrophilic ligand which contains a five

hydroxyl groups. A similar trend is observed in the NMR relaxometry experiment when comparing both silica (see below).

3.2.3 Water intrusion/extrusion measurements

For AMT C8, AMT C18, and AMT PFP, capillary condensation was not observed at relative pressures below bulk coexistence ($p p_0^{-1} < 1$) as expected due to the hydrophobic nature ($\theta > 90^{\circ}$) of the surface functionalization. To obtain the effective contact angles, a novel methodology based on water intrusion was applied to the three SPMs. During water intrusion, similar to mercury intrusion, hydraulic pressure is applied on water to form a liquid phase inside the pores. The intrusion/extrusion curves are shown in Figure 6. In this case, hydraulic pressure (p_h) is applied to intrude the non-wetting liquid water into the pores of a porous material. The contact angle can be determined from the Washburn equation (eq. 3) [21], if the pore radius (r) is known (from Ar adsorption measurements):

$$p_h = -\frac{2\gamma_{lv}cos\theta}{r} \tag{3}$$

where γ_{lv} is the surface tension, r the pore radius and θ the effective contact angle. For highly curved surfaces, the surface tension may depend on the curvature. However, molecular simulations indicate that the curvature effect is negligible for bubbles with a radius larger than 5 nm [47], in agreement with older works indicating that such corrections are only needed when the curvature radius approaches molecular dimensions [48,49].

After accounting for compressibility (see section 2.3), a clear and distinct intrusion step with a successive plateau is obtained for the three hydrophobic SPMs. The intrusion step occurs at 24.6 MPa for AMT C8, 24.4 MPa for AMT C18, and 17.5 MPa for AMT PFP. Interestingly, while we observe extrusion of water from the pores at 3.1 and 1.3 MPa for AMT C8 and AMT C18, respectively, no extrusion is observed for AMT PFP when returning to ambient pressure. Subsequent cycles on AMT PFP did not show any intrusion into the mesopores. Pioneering work from Fadeev et. al [50] on several hydrophobic silicas showed that for C8 silicas (with a similar pore diameter) the intrusion and extrusion pressures were at 23.0 and 3.1 MPa, respectively, in great agreement with our results here. Their work also contained water intrusion measurements on silicas functionalized with short chain, fluorinated alkyl groups. Here, similar to our results, no extrusion was observed. It has to be noted, that their functional groups did not include an aromatic ring as it is present for AMT PFP.

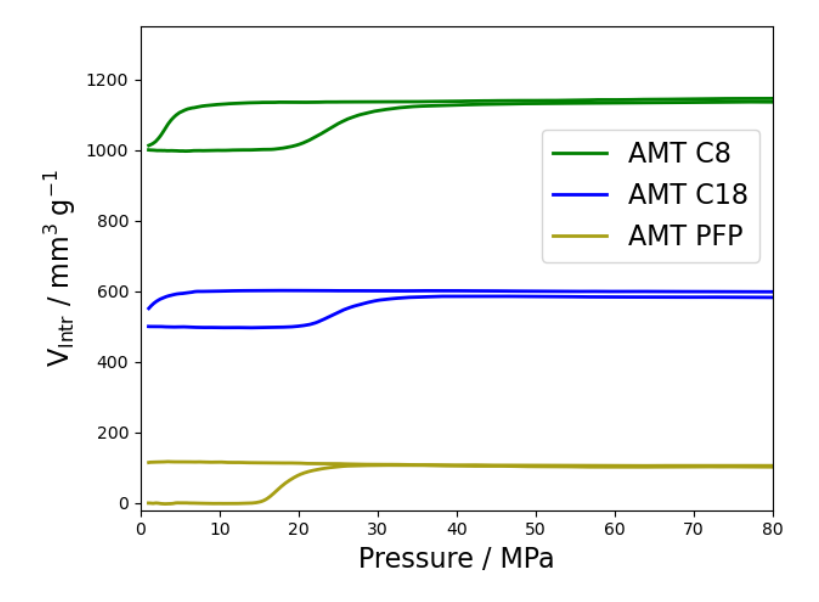


Figure 6: Water intrusion/extrusion curves on AMT PFP, AMT C18 and AMT C8 for the uncorrected and the compressibility corrected case. AMT C18 and AMT C8 are shifted for 500 and 1000 mm³ g⁻¹ for better visibility.

The corrected intrusion curve can then be used to obtain the effective contact angles. This is done by evaluating the pore size distribution of the water intrusion branch with the Washburn equation (eq. 3) and fitting it to the benchmark distribution obtained by the argon adsorption using the contact angle as a variable. In analogy to the Washburn equation, the BJH approach (modified Kelvin equation) is applied to the desorption branch of the argon isotherm to obtain the corresponding pore size distribution. The obtained fits are shown in Figure 7. The pore size distributions obtained from the water intrusion measurements are slightly broader than those obtained by the argon data. This might reflect differences of the orientational and conformational distribution of the ligands for the three SPMs at these experimental conditions (highly pressurized water at 298 K and argon vapor at 87 K). The estimates of the effective contact angles of 119° and 120° are very similar for *AMT C8* and *AMT C18*.

This finding is in good correspondence to experiments done by Fadeev and coworkers, showing no significant effect of alkyl chain length on the effective contact angle of water for hydrophobized flat silicon surfaces. Here, they measured a macroscopic droplet and reported an advancing contact angle of 110° [51]. Lefevre et. al. [52] have reported also 120° for a MCM-41 functionalized with *n*-octyl-dimethylchlorosilane (C8) while using a water intrusion experimental setup and the Washburn equation (eq 3). *AMT PFP* with 114° exhibits a lower effective contact angle indicating the slightly less hydrophobic nature of the samples. In previous work [50], it was also observed that fluorinated hydrocarbons provide a less hydrophobic surface than non-fluorinated hydrocarbon functionalized surfaces. Additionally, the aromatic nature of the PFP ligands might contribute to a slightly higher polarity and thus to the lower effective contact angle of water.

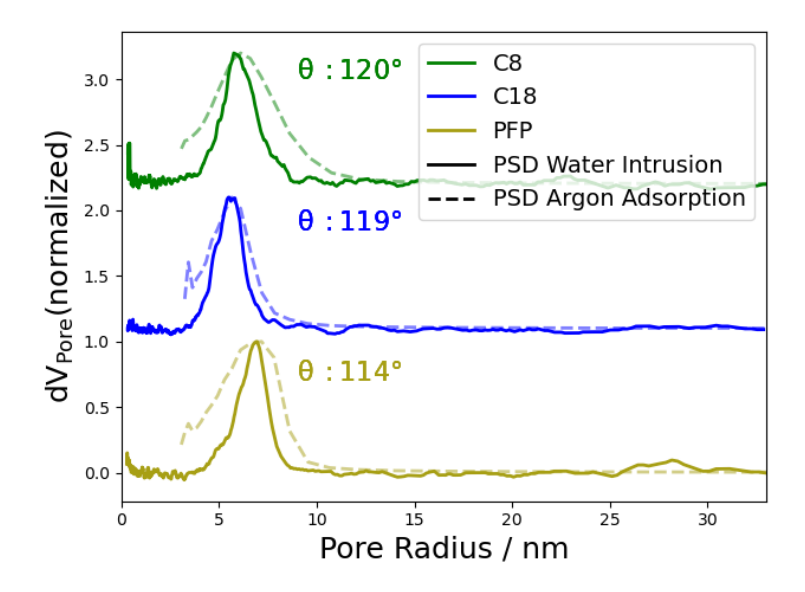


Figure 7: Fit of pore size distribution obtained via the Washburn equation and the water intrusion curves using the contact angle as a variable to the pore size distribution obtained from the argon isotherm via the BJH method (modified Kelvin equation).

3.2.4 NMR relaxometry

NMR relaxometry is used to calculate the $T_{1,ads,film}$ / $T_{2,ads,film}$ -ratio for AMT silica, AMT glycan, and AMT C18 in order to investigate and quantify the surface chemistry. This method is based on the different relaxation behavior of molecules in contact with a surface compared to those in the bulk phase (or "free" liquid). Molecules in a layer near a (nanoporous) particle surface exhibit a much shorter relaxation time compared to the bulk fluid due to the reduction of rotational and translational molecular mobility of the adsorbed molecules [53]. The specific surface area as well as the surface chemistry of the material under study affects the relaxation time reduction. In the fast diffusion regime, the relaxation time can be described by the two-fraction-fast-exchange-model [54]:

$$\frac{1}{T_i} = \frac{1}{T_{i,bulk}} + k_{a,i} \frac{S \cdot V_{solid}}{V_{liquid}} \tag{4}$$

Here, T_i is the relaxation time of the porous material immersed in the liquid phase, $T_{i,bulk}$ is the relaxation time of the pure bulk liquid with i=1 for spin-lattice and i=2 for spin-spin relaxation. S is the specific surface area of the porous material under study, V_{liquid} is the volume of liquid in the sample and V_{solid} the volume of the nanoporous material under study. The parameter $k_{a,i}$ is the specific surface relaxivity and is a measure for the relaxation time reduction of molecules adsorbed at the particle surface compared to the bulk liquid:

$$k_{a,i} = \lambda_{ads.film} \cdot \rho_{solid} \cdot \left(\frac{1}{T_{i,ads.film}} - \frac{1}{T_{i,bulk}}\right)$$
 (5)

 $\lambda_{ads.film}$ is a measure for the effective thickness of the adsorbed phase, $T_{i,ads.film}$ the corresponding relaxation time of the adsorbed phase and ρ_{solid} the skeletal density of the material under study. Please note, this definition can be transformed to the definition of surface relaxivity $\rho_i = \frac{\lambda_{ads.film}}{T_{i,ads.film}}$ by Davis et al. [55] assuming that $T_{i,ads.film} \ll T_{i,bulk}$ and by shifting the skeletal density from eq. 3 to eq. 2.

Fairhurst et al. showed a dependence between the T_2 reduction and the interaction strength of different fluids in contact with the surface of zinc oxide powders [56]. However, the relaxation time is affected by surface chemistry as well as surface area and confinement effects and the

relaxation time can therefore not be interpreted in a straightforward way for the quantification of the surface chemistry of different nanoporous materials. D'Agostino et al. suggested to use the ratio of spin-lattice to spin-spin relaxation time as a measure for the effective interaction strength between liquids and porous materials surfaces [25–27]. They found a linear correlation between the inverse relaxation time ratio $(-T_2/T_1)$ and the desorption enthalpy determined from TPD measurements for water saturated samples [28–30]. Our previous experiments confirmed that the T_1/T_2 ratio can be coupled with the interaction strength of adsorbates on surfaces [22]. However, the effect of the specific surface area on T_1 is less pronounced compared to T_2 , i.e. a stronger relaxation time reduction can be observed for T_2 [22,31]. To neglect the effect of the T_1/T_2 ratio on textural properties, we suggest to use the ratio of specific surface relaxivities $k_{a,2}/k_{a,1}$, which can be simplified to the ratio of relaxation times in the adsorbed liquid film $T_{1,ads,film}/T_{2,ads,film}$ assuming that $T_{i,ads,film} \ll T_{i,bulk}$:

$$\frac{k_{a,2}}{k_{a,1}} = \frac{\lambda_{Ads} \cdot \rho_{Solid} \cdot (\frac{1}{T_{2,ads.film}} - \frac{1}{T_{2,Bulk}})}{\lambda_{Ads} \cdot \rho_{Solid} \cdot (\frac{1}{T_{1,ads.film}} - \frac{1}{T_{1,Bulk}})} \approx \frac{T_{1,ads.film}}{T_{2,ads.film}}$$

$$(6)$$

For the investigation of the surface chemistry by NMR relaxometry, first T_1 and T_2 calibration lines are generated to calculate the specific surface relaxivities by using the bulk water relaxation times and the relaxation times of water saturated samples (Figure 8a,b). The specific surface area on the x-axis of the calibration plots is determined from Ar 87 K adsorption (Table 1).

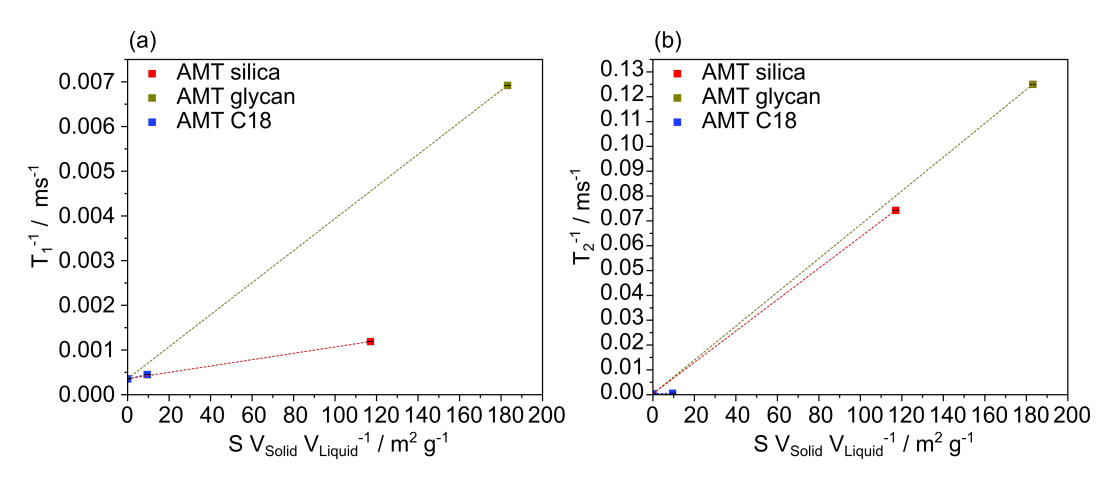


Figure 8: (a) T_1 and (b) T_2 calibration lines for AMT silica, AMT glycan and AMT C18, the slope of the linear lines corresponds to the specific surface relaxivity $k_{a,1}$ and $k_{a,2}$

Figure 9a shows the ratio of the specific surface relaxivities $k_{a,2}/k_{a,1}$, which is equal to the $T_{1,ads,film}/T_{2,ads,film}$ -ratio. One can clearly see that the interaction strength between water and AMT silica is most favorable, which is in line with the observations of the water vapor adsorption experiments. The hydrophobic nature of AMT C18 is clearly represented in the small $T_{1,ads,film}/T_{2,ads,film}$ -ratio, which agrees well with the large contact angle determined from water intrusion experiments. The three investigated SPMs vary mainly in their surface functional groups, textural properties such as the pore size distribution are comparable. Hence, we can neglect confinement effects that could affect the specific surface relaxivities in this case. However, future studies are required to systematically investigate how pore size and geometry affect the specific spin-lattice and spin-spin surface relaxivities and hence, the $T_{1,ads,film}/T_{2,ads,film}$ -ratio.

3.2.5 Comparison of water vapor adsorption, water intrusion and NMR relaxometry measurements

The comprehensive surface chemistry assessment in this study is based on the application of water vapor adsorption, water intrusion/extrusion, and NMR relaxometry. The correlation of the water contact angle with the $T_{1,ads,film}/T_{2,ads,film}$ -ratio determined with NMR relaxometry is shown in Figure 99a. We can clearly see that the most hydrophilic sample is AMT silica as it shows a contact angle close to zero and the highest $T_{1,ads,film}/T_{2,ads,film}$ -ratio. The hydrophobic nature of AMT C18 is reflected in the large contact angle of ≈ 120 ° and the comparatively small $T_{1,ads,film}/T_{2,ads,film}$ ratio. Indeed, a linear correlation can be found between the contact angle and the inverse relaxation time ratio $-T_{2,ads,film}/T_{1,ads,film}$ (Figure 99b), clearly indicating that both values can be used complementary to analyze the wettability and surface chemistry characteristics of porous materials. NMR relaxometry might be advantageous for fast surface chemistry characterization due to shorter measurement times compared to water vapor adsorption experiments, i.e., the measurement of T_1 and T_2 only takes a couple of minutes.

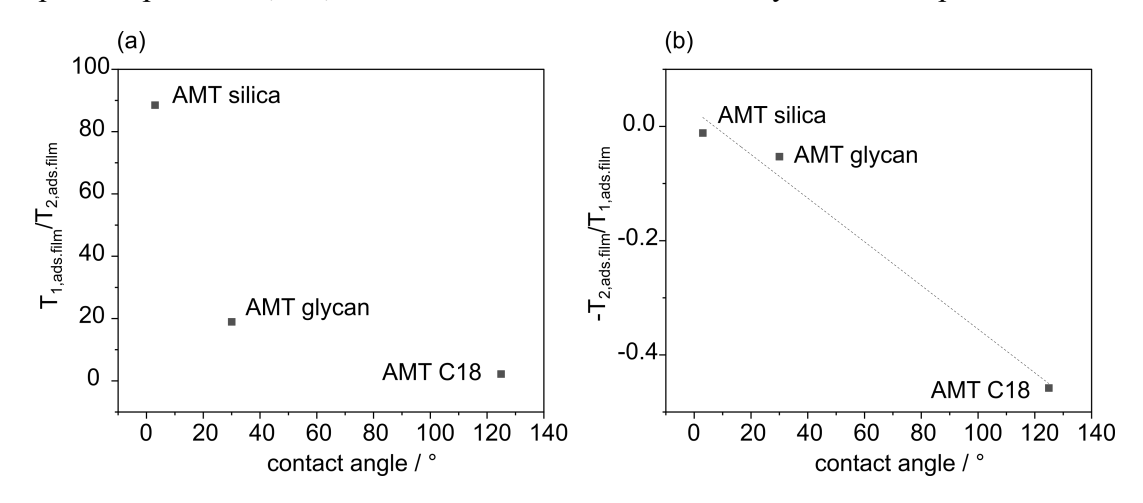


Figure 9: Correlation between the contact angle determined with water vapor adsorption and water intrusion, respectively with (a) the $T_{1,ads,film}/T_{2,ads-film}$ ratio and (b) the negative inverse relaxation time ratio $-T_{2,ads,film}/T_{1,ads,film}$

4 Conclusions

This study presents the comprehensive textural and surface chemistry characterization of porous silica particles, modified with different bonded ligands, by utilizing a combination of adsorptives, which completely wet the surface independent of its surface chemistry (e.g., Ar 87 K) and adsorptives, which are wetting, partially wetting or non-wetting depending on the surface chemistry (e.g., water). Water vapor adsorption as well as NMR relaxometry clearly confirm that AMT silica and AMT glycan are hydrophilic, with the former possessing a slightly smaller contact angle and higher $T_{1,ads.film}/T_{2,ads.film}$ ratio than AMT glycan. In contrast, the hydrophobic nature of the AMT C8, AMT C18 and AMT PFP stationary-phase materials is confirmed by water vapor adsorption experiments and further quantified by water intrusion and NMR relaxometry measurements. Indeed, we find a linear correlation between the contact angle determined from water vapor adsorption and water intrusion experiments with the negative inverse relaxation time ratio $-T_{2,ads.film}/T_{1,ads.film}$. Further, NMR relaxometry is shown to be a powerful and unique tool for the fast assessment of surface chemistry as T_1 and T_2 measurements only take between 3 and 20 min. ¹H MAS NMR spectroscopy allows to estimate the number of surface-grafted functional groups, reveals the presence and the number of endcapping groups for those samples with well-resolved spectral features and allows to visualize residual surface-bound water and silanol groups in hydrogen bonding, present on the surface after activation under mild conditions.

The detailed understanding of the textural and surface chemistry is crucial for material synthesis and process design and have a direct impact into the transport properties, selectivity to certain

compounds and separation efficiency of chromatographic separation processes etc. Our work demonstrates for the first time that water vapor adsorption experiments and the novel water intrusion technique coupled with NMR relaxometry can be used as complementary techniques to quantitatively analyze the wettability behavior and surface chemistry of nanoporous materials.

5 Acknowledgements

The work was supported by the Deutsche Forschungsgemeinschaft (DFG, German Research Foundation)—Project-ID 416229255 – SFB 1411 as well as Project-ID 431791331 - SFB 1452. The molecular simulation work was supported by the Chemical Measurement & Imaging program, with co-funding from the Interfacial Engineering program, of the National Science Foundation (CHE-2003246).

6 References

- [1] H. Qiu, X. Liang, M. Sun, S. Jiang, Development of silica-based stationary phases for high-performance liquid chromatography, Anal. Bioanal. Chem. 399 (2011) 3307–3322. https://doi.org/10.1007/s00216-010-4611-x.
- [2] J. Zhao, F. Gao, Y. Fu, W. Jin, P. Yang, D. Zhao, Biomolecule separation using large pore mesoporous SBA-15 as a substrate in high performance liquid chromatography, Chem. Commun. (2002) 752–753. https://doi.org/10.1039/B110637F.
- [3] C.P. Tripp, M.L. Hair, Reaction of Methylsilanols with Hydrated Silica Surfaces: The Hydrolysis of Trichloro-, Dichloro-, and Monochloromethylsilanes and the Effects of Curing, Langmuir. 11 (1995) 149–155. https://doi.org/10.1021/la00001a027.
- [4] S. Liu, H. Xu, J. Yu, D. Li, M. Li, X. Qiao, X. Qin, H. Yan, Novel imidazolium-embedded N,N-dimethylaminopropyl-functionalized silica-based stationary phase for hydrophilic interaction/reversed-phase mixed-mode chromatography, Anal. Bioanal. Chem. 407 (2015) 8989–8997. https://doi.org/10.1007/s00216-015-9064-9.
- [5] Y. Wang, M. Tian, W. Bi, K.H. Row, Application of Ionic Liquids in High Performance Reversed-Phase Chromatography, Int. J. Mol. Sci. 10 (2009) 2591–2610. https://doi.org/10.3390/ijms10062591.
- [6] T.L. Ascah, K.M.R. Kallury, C.A. Szafranski, S.D. Corman, F. Liu, Characterization and High Performance Liquid Chromatographic Evaluation of a New Amide-Functionalized Reversed Phase Column, J. Liq. Chromatogr. Relat. Technol. 19 (1996) 3049–3073. https://doi.org/10.1080/10826079608015125.
- [7] Adsorption, X-ray diffraction, photoelectron, and atomic emission spectroscopy benchmark studies for the eighth industrial fluid properties simulation challenge Richard B Ross, David B Aeschliman, Riaz Ahmad, John K Brennan, Myles L Brostrom, Kevin A Frankel, Jonathan D Moore, Joshua D Moore, Raymond D Mountain, Derrick M Poirier, Matthias Thommes, Vincent K Shen, Nathan E Schultz, Daniel W Siderius, Kenneth D Smith, 2016, (n.d.). https://journals.sagepub.com/doi/10.1177/0263617415619541 (accessed April 12, 2023).
- [8] T.J. Horr, J. Ralston, R.St.C. Smart, The use of contact angle measurements to quantify the adsorption density and thickness of organic molecules on hydrophilic surfaces, Colloids Surf. Physicochem. Eng. Asp. 97 (1995) 183–196. https://doi.org/10.1016/0927-7757(95)03090-Z.

- [9] T. Dang-Vu, J. Hupka, CHARACTERIZATION OF POROUS MATERIALS BY CAPILLARY RISE METHOD, (n.d.).
- [10] R.N. Lamb, D.N. Furlong, Controlled wettability of quartz surfaces, J. Chem. Soc. Faraday Trans. 1 Phys. Chem. Condens. Phases. 78 (1982) 61–73. https://doi.org/10.1039/F19827800061.
- [11] M. Thommes, J. Morell, K.A. Cychosz, M. Fröba, Combining Nitrogen, Argon, and Water Adsorption for Advanced Characterization of Ordered Mesoporous Carbons (CMKs) and Periodic Mesoporous Organosilicas (PMOs), Langmuir. 29 (2013) 14893–14902. https://doi.org/10.1021/la402832b.
- [12] M. Thommes, S. Mitchell, J. Pérez-Ramírez, Surface and Pore Structure Assessment of Hierarchical MFI Zeolites by Advanced Water and Argon Sorption Studies, J. Phys. Chem. C. 116 (2012) 18816–18823. https://doi.org/10.1021/jp3051214.
- [13] M. Thommes, C. Morlay, R. Ahmad, J.P. Joly, Assessing surface chemistry and pore structure of active carbons by a combination of physisorption (H2O, Ar, N2, CO2), XPS and TPD-MS, Adsorption. 17 (2011) 653–661. https://doi.org/10.1007/s10450-011-9360-4
- [14] R.O. David, J. Fahrni, C. Marcolli, F. Mahrt, D. Brühwiler, Z.A. Kanji, The role of contact angle and pore width on pore condensation and freezing, Atmospheric Chem. Phys. 20 (2020) 9419–9440. https://doi.org/10.5194/acp-20-9419-2020.
- [15] S. Inagaki, Y. Fukushima, Adsorption of water vapor and hydrophobicity of ordered mesoporous silica, FSM-16, Microporous Mesoporous Mater. 21 (1998) 667–672. https://doi.org/10.1016/S1387-1811(98)00075-4.
- [16] V. Kocherbitov, V. Alfredsson, Hydration of MCM-41 Studied by Sorption Calorimetry, J. Phys. Chem. C. 111 (2007) 12906–12913. https://doi.org/10.1021/jp072474r.
- [17] S. Saliba, P. Ruch, W. Volksen, T.P. Magbitang, G. Dubois, B. Michel, Combined influence of pore size distribution and surface hydrophilicity on the water adsorption characteristics of micro- and mesoporous silica, Microporous Mesoporous Mater. 226 (2016) 221–228. https://doi.org/10.1016/j.micromeso.2015.12.029.
- [18] T.H. Muster, C.A. Prestidge, R.A. Hayes, Water adsorption kinetics and contact angles of silica particles, Colloids Surf. Physicochem. Eng. Asp. 176 (2001) 253–266. https://doi.org/10.1016/S0927-7757(00)00600-2.
- [19] T. Takei, A. Yamazaki, T. Watanabe, M. Chikazawa, Water Adsorption Properties on Porous Silica Glass Surface Modified by Trimethylsilyl Groups, J. Colloid Interface Sci. 188 (1997) 409–414. https://doi.org/10.1006/jcis.1997.4777.
- [20] H. Huang, T. Oike, F. Watanabe, Y. Osaka, N. Kobayashi, M. Hasatani, Development research on composite adsorbents applied in adsorption heat pump, Appl. Therm. Eng. 30 (2010) 1193–1198. https://doi.org/10.1016/j.applthermaleng.2010.01.036.
- [21] S. Lowell, J.E. Shields, M.A. Thomas, M. Thommes, Characterisation of porous solids and Powders: Surface Area, Pore Size and Density, Kluwer Academic Publishers, 2004.
- [22] C. Schlumberger, L. Sandner, A. Michalowski, M. Thommes, Reliable Surface Area Assessment of Wet and Dry Nonporous and Nanoporous Particles: Nuclear Magnetic Resonance Relaxometry and Gas Physisorption, Langmuir. (2023) acs.langmuir.2c03337. https://doi.org/10.1021/acs.langmuir.2c03337.
- [23] R.L. Kleinberg, S.A. Farooqui, M.A. Horsfield, T1/T2 Ratio and Frequency Dependence of NMR Relaxation in Porous Sedimentary Rocks, J. Colloid Interface Sci. 158 (1993) 195–198. https://doi.org/10.1006/jcis.1993.1247.
- [24] B. Maillet, R. Sidi-Boulenouar, P. Coussot, Dynamic NMR Relaxometry as a Simple Tool for Measuring Liquid Transfers and Characterizing Surface and Structure Evolution in Porous Media, Langmuir. 38 (2022) 15009–15025. https://doi.org/10.1021/acs.langmuir.2c01918.

- [25] C. D'Agostino, G.L. Brett, P.J. Miedziak, D.W. Knight, G.J. Hutchings, L.F. Gladden, M.D. Mantle, Understanding the Solvent Effect on the Catalytic Oxidation of 1,4-Butanediol in Methanol over Au/TiO2 Catalyst: NMR Diffusion and Relaxation Studies, Chem. Eur. J. 18 (2012) 14426–14433. https://doi.org/10.1002/chem.201201922.
- [26] C. D'Agostino, T. Kotionova, J. Mitchell, P.J. Miedziak, D.W. Knight, S.H. Taylor, G.J. Hutchings, L.F. Gladden, M.D. Mantle, Solvent Effect and Reactivity Trend in the Aerobic Oxidation of 1,3-Propanediols over Gold Supported on Titania: NMR Diffusion and Relaxation Studies, Chem. Eur. J. 19 (2013) 11725–11732. https://doi.org/10.1002/chem.201300502.
- [27] C. D'Agostino, M.R. Feaviour, G.L. Brett, J. Mitchell, A.P.E. York, G.J. Hutchings, M.D. Mantle, L.F. Gladden, Solvent inhibition in the liquid-phase catalytic oxidation of 1,4-butanediol: understanding the catalyst behaviour from NMR relaxation time measurements, Catal. Sci. Technol. 6 (2016) 7896–7901. https://doi.org/10.1039/C6CY01458E.
- [28] C. D'Agostino, J. Mitchell, M.D. Mantle, L.F. Gladden, Interpretation of NMR Relaxation as a Tool for Characterising the Adsorption Strength of Liquids inside Porous Materials, Chem. Eur. J. 20 (2014) 13009–13015. https://doi.org/10.1002/chem.201403139.
- [29] N. Robinson, C. Robertson, L.F. Gladden, S.J. Jenkins, C. D'Agostino, Direct Correlation between Adsorption Energetics and Nuclear Spin Relaxation in a Liquid-saturated Catalyst Material, ChemPhysChem. 19 (2018) 2472–2479. https://doi.org/10.1002/cphc.201800513.
- [30] N. Robinson, P. Bräuer, A.P.E. York, C. D'Agostino, Nuclear spin relaxation as a probe of zeolite acidity: a combined NMR and TPD investigation of pyridine in HZSM-5, Phys. Chem. Chem. Phys. 23 (2021) 17752–17760. https://doi.org/10.1039/D1CP01515J.
- [31] A. Delville, M. Letellier, Structure and Dynamics of Simple Liquids in Heterogeneous Condition: An NMR Study of the Clay-Water Interface, Langmuir. 11 (1995) 1361–1367. https://doi.org/10.1021/la00004a050.
- [32] B.M. Wagner, S.A. Schuster, B.E. Boyes, T.J. Shields, W.L. Miles, M.J. Haynes, R.E. Moran, J.J. Kirkland, M.R. Schure, Superficially Porous Particles with 1000 Å Pores for Large Biomolecule High Performance Liquid Chromatography and Polymer Size Exclusion Chromatography, J. Chromatogr. A. 1489 (2017) 75–85. https://doi.org/10.1016/j.chroma.2017.01.082.
- [33] E.W. Lemmon, THERMOPHYSICAL PROPERTIES OF FLUIDS, NIST. (2009). https://www.nist.gov/publications/thermophysical-properties-fluids (accessed April 12, 2023).
- [34] G. Bodenhausen, R. Freeman, D.L. Turner, Suppression of artifacts in two-dimensional J spectroscopy, J. Magn. Reson. 1969. 27 (1977) 511–514. https://doi.org/10.1016/0022-2364(77)90016-6.
- [35] M. Robin Bendall, R.E. Gordon, Depth and refocusing pulses designed for multipulse NMR with surface coils, J. Magn. Reson. 53 (1983) 365–385. https://doi.org/10.1016/0022-2364(83)90211-1.
- [36] D.G. Cory, W.M. Ritchey, Suppression of signals from the probe in bloch decay spectra, J. Magn. Reson. 1969. 80 (1988) 128–132. https://doi.org/10.1016/0022-2364(88)90064-9.
- [37] D. Massiot, F. Fayon, M. Capron, I. King, S. Le Calvé, B. Alonso, J.-O. Durand, B. Bujoli, Z. Gan, G. Hoatson, Modelling one- and two-dimensional solid-state NMR spectra, Magn. Reson. Chem. 40 (2002) 70–76. https://doi.org/10.1002/mrc.984.
- [38] C.C. Collados, C. Huber, J. Söllner, J.-P. Grass, A. Inayat, R. Durdyyev, A. Smith, D. Wisser, M. Hartmann, M. Thommes, Quantitative Assessment of Hydrophilicity/Hydrophobicity in Mesoporous Silica by combining Adsorption, Liquid

- Intrusion and solid-state NMR spectroscopy, (2023). https://doi.org/10.26434/chemrxiv-2023-tgk5g.
- [39] M. Thommes, K. Kaneko, A.V. Neimark, J.P. Olivier, F. Rodriguez-Reinoso, J. Rouquerol, K.S.W. Sing, Physisorption of gases, with special reference to the evaluation of surface area and pore size distribution (IUPAC Technical Report), Pure Appl. Chem. 87 (2015). https://doi.org/10.1515/pac-2014-1117.
- [40] C. Schlumberger, M. Thommes, Characterization of Hierarchically Ordered Porous Materials by Physisorption and Mercury Porosimetry—A Tutorial Review, Adv. Mater. Interfaces. 8 (2021) 2002181. https://doi.org/10.1002/admi.202002181.
- [41] K.A. Cychosz, R. Guillet-Nicolas, J. García-Martínez, M. Thommes, Recent advances in the textural characterization of hierarchically structured nanoporous materials, Chem. Soc. Rev. 46 (2017) 389–414. https://doi.org/10.1039/C6CS00391E.
- [42] F. Kleitz, F. Bérubé, R. Guillet-Nicolas, C.-M. Yang, M. Thommes, Probing Adsorption, Pore Condensation, and Hysteresis Behavior of Pure Fluids in Three-Dimensional Cubic Mesoporous KIT-6 Silica, (2010). https://doi.org/10.1021/jp909836v.
- [43] R. Guillet-Nicolas, F. Bérubé, M. Thommes, M.T. Janicke, F. Kleitz, Selectively Tuned Pore Condensation and Hysteresis Behavior in Mesoporous SBA-15 Silica: Correlating Material Synthesis to Advanced Gas Adsorption Analysis, J. Phys. Chem. C. 121 (2017) 24505–24526. https://doi.org/10.1021/acs.jpcc.7b06745.
- [44] C. Schlumberger, C. Scherdel, M. Kriesten, P. Leicht, A. Keilbach, H. Ehmann, P. Kotnik, G. Reichenauer, M. Thommes, Reliable Surface Area Determination of Porous Materials: Small-Angle X-ray Scattering and Gas Physisorption, Microporous Mesoporous Mater. to be published (2021).
- [45] C.E. Bronnimann, R.C. Zeigler, G.E. Maciel, Proton NMR study of dehydration of the silica gel surface, J. Am. Chem. Soc. 110 (1988) 2023–2026. https://doi.org/10.1021/ja00215a001.
- [46] L.T. Zhuravlev, The surface chemistry of amorphous silica. Zhuravlev model, Colloids Surf. Physicochem. Eng. Asp. 173 (2000) 1–38. https://doi.org/10.1016/S0927-7757(00)00556-2.
- [47] J.L. Chen, B. Xue, K. Mahesh, J.I. Siepmann, Molecular Simulations Probing the Thermophysical Properties of Homogeneously Stretched and Bubbly Water Systems, J. Chem. Eng. Data. 64 (2019) 3755–3771. https://doi.org/10.1021/acs.jced.9b00284.
- [48] L.R. Fisher, J.N. Israelachvili, Determination of the Capillary pressure in menisci of molecular dimensions, Chem. Phys. Lett. 76 (1980) 325–328. https://doi.org/10.1016/0009-2614(80)87033-3.
- [49] V.B. Fenelonov, G.G. Kodenyov, V.G. Kostrovsky, On the Dependence of Surface Tension of Liquids on the Curvature of the Liquid-Vapor Interface, J. Phys. Chem. B. 105 (2001) 1050–1055. https://doi.org/10.1021/jp9929972.
- [50] A.Y. Fadeev, V.A. Eroshenko, Study of Penetration of Water into Hydrophobized Porous Silicas, J. Colloid Interface Sci. 187 (1997) 275–282. https://doi.org/10.1006/jcis.1996.4495.
- [51] Trialkylsilane Monolayers Covalently Attached to Silicon Surfaces: Wettability Studies Indicating that Molecular Topography Contributes to Contact Angle Hysteresis | Langmuir, (n.d.). https://pubs.acs.org/doi/10.1021/la9814860 (accessed April 12, 2023).
- [52] B. Lefevre, A. Saugey, J.L. Barrat, L. Bocquet, E. Charlaix, P.F. Gobin, G. Vigier, Intrusion and extrusion of water in hydrophobic mesopores, J. Chem. Phys. 120 (2004) 4927–4938. https://doi.org/10.1063/1.1643728.
- [53] B.E. Kinn, T.R. Myers, A.M. Allgeier, Surface enhanced nuclear magnetic resonance relaxation mechanisms and their significance in chemical engineering applications, Curr. Opin. Chem. Eng. 24 (2019) 115–121. https://doi.org/10.1016/j.coche.2019.03.010.

- [54] K.R. Brownstein, C.E. Tarr, Importance of classical diffusion in NMR studies of water in biological cells, Phys. Rev. A. 19 (1979) 2446–2453. https://doi.org/10.1103/PhysRevA.19.2446.
- [55] P.J. Davis, D.P. Gallegos, D.M. Smith, Rapid surface area determination via NMR spinlattice relaxation measurements, Powder Technol. 53 (1987) 39–47. https://doi.org/10.1016/0032-5910(87)80123-7.
- [56] D. Fairhurst, R. Sharma, S. Takeda, T. Cosgrove, S.W. Prescott, Fast NMR relaxation, powder wettability and Hansen Solubility Parameter analyses applied to particle dispersibility, Powder Technol. 377 (2021) 545–552. https://doi.org/10.1016/j.powtec.2020.09.002.